Progress In Electromagnetics Research, Vol. 131, 153–167, 2012

COMPLEX PHOTONIC BAND STRUCTURES IN A PHOTONIC CRYSTAL CONTAINING LOSSY SEMICONDUCTOR INSB

T.-W. Chang[1], J.-J. Wu[2], and C.-J. Wu[3, *]

[1]Graduate Institute of Electro-Optical Engineering, Chang Gung University, Tao-Yuan 333, Taiwan, R.O.C.

[2]Department of Electrical Engineering, Chung Hua University, Hsinchu 300, Taiwan, R.O.C.

[3]Institute of Electro-Optical Science and Technology, National Taiwan Normal University, Taipei 116, Taiwan, R.O.C.

Abstract—In this work, complex photonic band structure (CPBS) in a semiconductor-dielectric photonic crystal (SDPC) operating at terahertz frequencies is theoretically investigated. The SDPC is air/(S/D)^N/air where the dielectric layer D is SiO_2, the semiconductor layer S is an intrinsic semiconductor InSb, and N is the number of periods. Using the experimental data for the strongly temperature-dependent plasma frequency and damping frequency for InSb, we calculate the CPBS for the infinite SDPC at distinct operating temperatures. The CPBS is then compared with the calculated transmittance, reflectance, and absorptance as well in the finite SDPC. Based on the calculated CPBS, the role played by the loss factor (damping frequency), in InSb is revealed. Additionally, from the calculated transmittance spectra, we further investigate the cutoff frequency for the SDPC. The dependences of cutoff frequency on the number of periods and the filling factor of semiconductor layer are numerically illustrated.

1. INTRODUCTION

It is known that there exist the photonic band gaps (PBGs) in a photonic crystal (PC). PBGs, which are analogous to the electronic band gaps (EBGs) in solids, arise from the Bragg scattering due to the

Received 29 July 2012, Accepted 23 August 2012, Scheduled 6 September 2012

* Corresponding author: Chien-Jang Wu (jasperwu@ntnu.edu.tw).

spatially periodic profile in the refractive index. PBGs are of technical use in designing the Bragg reflectors (BRs) that play an important role in solid state laser systems [1–3]. Engineering PBGs to realize other possible photonic devices, including resonators, polarizer, filters, beam splitter, and waveguides are also available [4–13].

In the early stage, PCs made of all dielectrics are of primary interest to the community because an all-dielectric PC possesses the so-called omnidirectional PBGs [14, 15]. At the same time, metal-dielectric photonic crystals (MDPCs) also attracted much attention since metals have a dispersive permittivity [16, 17]. MDPCs have some superior features than all-dielectric PCs. For example, they have wider PBGs, and they can be used to enhance the transmission at frequency below the plasma frequency, i.e., at visible frequency region [18, 19].

In addition to MDPCs, another type of PC containing semiconducting materials was studied by Halevi and Ramos-Mendieta [20]. The use of semiconductor can make the PBGs tunable. The tunability comes from the fact that the permittivity of semiconductor can be changed by the carrier concentration $\tilde{N}$ which could be a function of temperature T. Thus, it is referred to as $\tilde{N}$-tuning or T-tuning [20]. Other tuning agents like electric field (E-tuning) and magnetic field (M-tuning) are also available. Examples of E-tuning are PCs containing liquid crystal [21–23]. PCs with a magnetic constituent are called the M-tuning [24–27]. Indeed, PCs with tunable PBGs are more attractive in the optoelectronic applications.

Recently, the photonic band structure (PBS) at terahertz (THz) for a semiconductor-dielectric photonic crystal (SDPC) containing intrinsic InSb has been investigated by Dai et al. [28]. However, the authors assume there is no loss in intrinsic InSb. This appears to be an apparent flaw since InSb is, indeed, a lossy medium at THz according the Palik's book [29]. Later, using lossy InSb as a defect layer in the Si/SiO_2 photonic crystal, the temperature- and concentration-dependent properties of defect mode have been investigated by Hung et al. [30]. Other related studies concentrate on the magnetic-field dependence of transmission properties in an extrinsic n type InSb-based photonic crystals [31, 32].

It is our main motivation, in this work, to properly include the loss factor in the permittivity of InSb in this SDPC, where S is intrinsic InSb and D is SiO_2. Due to the inherent loss in InSb, it is found that the photonic band structure of an SDPC should be complex, i.e., a complex Bloch wave number should exist in both the PBGs and passbands. To compare the calculated PBGs, we also give the plots of transmittance, reflectance, and absorptance spectra as well. Finally, we study the fundamental information about the cutoff frequency for such an SDPC. The dependences of cutoff frequency on the number of periods and the thickness ratio of the two constituent layers are also illustrated.

The format of this paper is given as follows: Section 1 gives the introduction. In Section 2, we describe the basic equations for the permittivity for the intrinsic InSb as well as the computational method. Section 3 is to present the numerical results and discussion. The conclusion is in Section 4.

2. BASIC EQUATIONS

Before we describe the transfer matrix method (TMM) for the calculation of PBS of SDPC, let us first mention the refractive index of InSb. In the THz frequency region, the dielectric constant of InSb, which is strongly dependent on the frequency as well as the temperature, can be modeled within the framework of the Drude-like model. Using the temporal part $\exp(j\omega t)$ for all fields, the expression of dielectric function is given by [20, 33],

$$\varepsilon_{\mathrm{InSb}}(\omega,T)=\varepsilon'_{\mathrm{InSb}}(\omega,T)-j\varepsilon''_{\mathrm{InSb}}(\omega,T)=\varepsilon_\infty-\frac{\omega_p^2}{\omega^2-j\gamma\omega}, \tag{1}$$

where ε_∞ is the high-frequency value, γ the damping frequency, and plasma frequency ω_p given by

$$\omega_p=2\pi f_p=\sqrt{\frac{\tilde{N}e^2}{m*\varepsilon_0}}, \tag{2}$$

where the strong temperature dependence of dielectric function arises from two factors. One is the intrinsic carrier density $\tilde{N}$ (in unit of m^{-3}) which is written by

$$\tilde{N}=\tilde{N}\left(T\right)=5.76\times10^{20}T^{3/2}\exp\left(-\frac{0.26}{2k_BT}\right). \tag{3}$$

Here, the number 0.26 is in unit of eV, e the electronic charge, ε_0 the permittivity of vacuum, k_B the Boltzmann constant, and m^* the effective mass of free carrier. The other is the damping frequency $\gamma=\gamma$ (T). With the complex dielectric function of InSb, the refractive index also is complex-valued and is the square root of the dielectric function, i.e., $n_{\mathrm{InSb}}=\sqrt{\varepsilon_{\mathrm{InSb}}}=n_R-jn_I$, where the imaginary part n_I indicates the extinction constant.

Although expression for the temperature-dependent carrier concentration in Eq. (3) is available, there is no available analytical expression for γ (T). Thus, it is awkward to directly use Eq. (1) to investigate the electromagnetic properies for the InSb-based photonic crystal. In a recent paper [28], the authors simply assume $\gamma = 0$ in calculating the THz PBS of InSb-SiO_2 SDPC. This assumption obviously is too simple to be correct at THz because the damping frequency is also a strong function of temperature [29]. Thus, in order to make a more realistic calculation, in this work, we shall adapt the experimental values for the temperature-dependent plasma frequency and the damping frequency, as listed in Table 1 [34]. With the inclusion of nonzero damping frequency, the calculated PBS is seen to be complex and is referred to as the so-called complex photonic band structure (CPBS). As will be seen later, in the CPBS, both the real and the imaginary parts of the Bloch wave vector can exist in the pass band or the stop band.

The CPBS for the infinite SDPC will be calculated within the framework of transfer matrix method (TMM) [35]. According to TMM, the CPBS can be computed by the single-period transfer matrix

$$\mathbf{M}_{\text{period}} = \begin{pmatrix} A & B \\ C & D \end{pmatrix} = \mathbf{M}_{\text{InSb}}\mathbf{M}_{\text{SiO}_2}, \tag{4}$$

where the transfer matrix in each layer is given by

$$\mathbf{M}_i = \mathbf{D}_i\mathbf{P}_i\mathbf{D}_i^{-1}, \quad i = 1(\text{InSb}) \text{ or } 2(\text{SiO}_2). \tag{5}$$

Here, the propagation matrix in layer i is expressed as

$$\mathbf{P}_i = \begin{pmatrix} \exp(jk_i d_i) & 0 \\ 0 & \exp(-jk_i d_i) \end{pmatrix}, \tag{6}$$

Table 1. The values of plasma frequency and damping frequency at several temperatures [34].

T (K)	$\omega_p/2\pi$ (THz)	$\gamma/2\pi$ (THz)	γ/ω_p
225	3.1	0.15	0.048
240	4.0	0.18	0.045
255	5.2	0.21	0.041
270	5.9	0.23	0.039
280	6.7	0.24	0.036
295	8.0	0.26	0.033
310	9.0	0.28	0.031
325	9.9	0.31	0.031

where $k_i = k_0 n_i = k_0\sqrt{\varepsilon_i}$ and d_i are the wave number and thickness in layer i, respectively, and $k_0 = \omega/c$ is the free-space wave number, in addition, the dynamical matrix in medium i is written by

$$\mathbf{D}_i = \begin{pmatrix} 1 & 1 \\ n_i & -n_i \end{pmatrix}. \tag{7}$$

The CPBS is then determined by the half trace of matrix given in Eq. (4), namely

$$\cos\left(K\Lambda\right) = \frac{1}{2}\left(A + D\right), \tag{8}$$

where $K = K_r - jK_i$ is the Bloch wave number, and $\Lambda = d_1 + d_2$ is spatial periodicity of the SDPC. The explicit expression for Eq. (8) can be further obtained to be

$$\cos(K\Lambda)=\cos(k_1 d_1)\cos(k_2 d_2)-\frac{1}{2}\left(\frac{n_1}{n_2}+\frac{n_2}{n_1}\right)\sin(k_1 d_1)\sin(k_2 d_2). \tag{9}$$

The solution for K as a function of frequency is the so-called photonic band structure. In the usual lossless PCs, solution for K will be purely real in the passband and conversely it will be purely imaginary in the photonic band gap. However, when the loss is incorporated, solution for K can be complex-valued for both the passband and the band gap (stop band).

In addition to K vs. frequency, the PBS can also be investigated by way of the transmittance Γ and reflectance R for the finite SDPC. Again, with the aid of TMM, the transmittance Γ and reflectance R are calculated through the following equations,

$$\Gamma = \left|\frac{1}{M_{11}}\right|^2, \quad R = \left|\frac{M_{21}}{M_{11}}\right|^2, \tag{10}$$

where M_{11} and M_{21} are the matrix elements of the total system matrix,

$$\mathbf{M}_{sys} = \begin{bmatrix} M_{11} & M_{12} \\ M_{21} & M_{22} \end{bmatrix} = \mathbf{D}_0^{-1}\left[\mathbf{D}_1\mathbf{P}_1\mathbf{D}_1^{-1}\mathbf{D}_2\mathbf{P}_2\mathbf{D}_2^{-1}\right]^N \mathbf{D}_0, \tag{11}$$

where $\mathbf{D}_0$ is the dynamical matrix of air and N the number of periods. The absorptance A is thus given by

$$A = 1 - \Gamma - R. \tag{12}$$

3. NUMERICAL RESULTS AND DISCUSSION

Let us first investigate the effect of damping frequency on the refractive index of InSb. With the use of Table 1 for the plasma and damping frequencies, the only material parameter in Eq. (1) is the high-frequency dielectric constant which is taken to be $\varepsilon_\infty = 15.68$ [20].

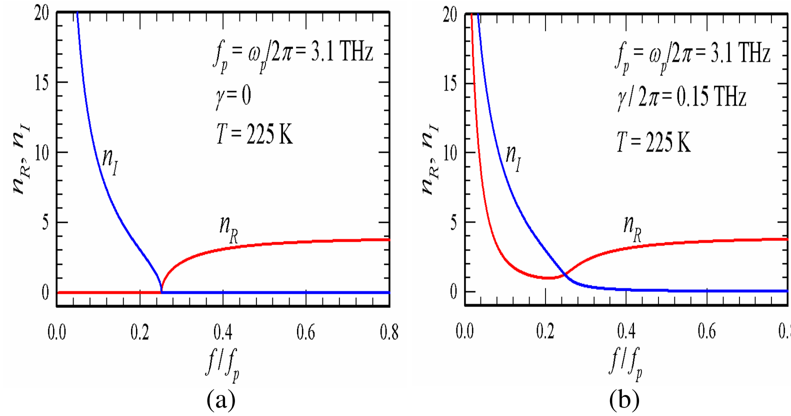

Figure 1. (a) Calculated refractive index of InSb without and with (b) damping frequency at a fixed temperature of 225 K.

The frequency-dependent real and imaginary parts of refractive index of InSb at $T = 225\,\text{K}$ are plotted in Figure 1. In the left panel, the damping frequency is turned off, $\gamma = 0$, whereas the right one is with a nonzero damping frequency of $\gamma = 2\pi \times 0.15\,\text{THz}$ selected from Table 1. It can be seen that the real and imaginary parts of the complex refractive index, n_R and n_I, intersect at $f_{int} = 0.25 f_p$, which is nearly the same for both the lossless and lossy cases. At $\gamma = 0$, the complex refractive index will become zero at f_{int}. The intersection point is far away the plasma frequency because the value of ε_∞ in the permittivity is much great than one. It is seen from the figure that, in the presence of loss factor, the real part n_R has been strongly modified at frequency lower than f_{int}. At frequency well above f_{int} the difference between $\gamma = 0$ and $\gamma > 0$ is very small. This is due to the negligible contribution from γ in Eq. (1) at frequency higher than f_{int}. Conclusively, the inclusion of damping frequency has a stronger influence in n_R than n_I, especially at low frequency regime.

Next, let us now enter the main issue of this work, the temperature-dependent CPBS for the InSb-SiO_2 SDPC. Here, the thicknesses of InSb and SiO_2 are denoted by d_1 and d_2, respectively. In Figure 2, we plot the CPBS at $T = 225\,\text{K}$. It can be seen that the first band gap (0–0.6 THz) shown in K_r plot is not entirely flat as in the usual lossless case. There is a small bending in K_r which is also reflected in the appearance of K_i in the same region. This small bending is ascribed to the small damping frequency at $T = 225\,\text{K}$. As seen Table 1, the damping frequency is $\gamma = 0.048\omega_p$, where $\omega_p = 2\pi \times 3.1\,\text{THz}$. Other than this bending, all the other photonic

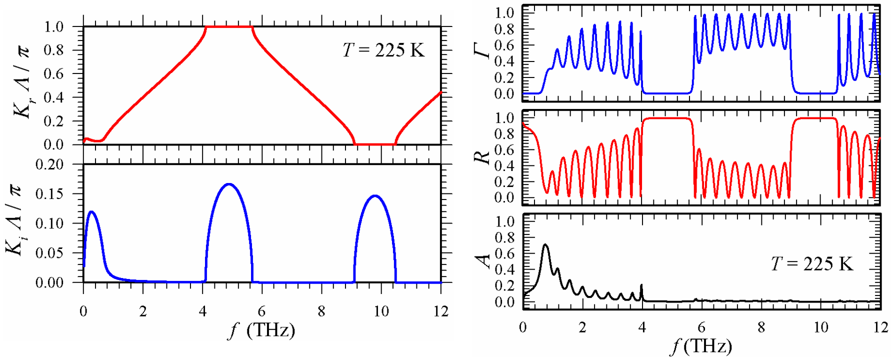

Figure 2. Calculated CPBS and Γ, R, and A at $T = 225\,\text{K}$ for Air/(InSb/SiO_2)^N/Air. Here, the thicknesses of InSb and SiO_2 layers are both equal to $d_1 = d_2 = 5\,\mu\text{m}$, and $N = 10$. The refractive index of SiO_2 is 2.2.

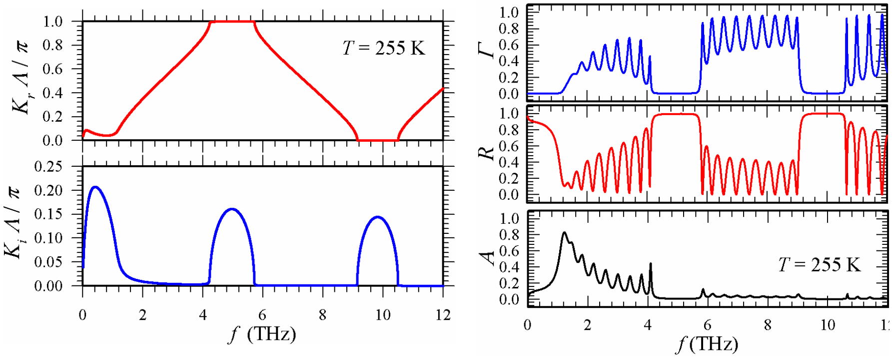

Figure 3. Calculated PBS and Γ, R, and A at $T = 255\,\text{K}$ for Air/(InSb/SiO_2)^N/Air. Here, the thicknesses of InSb and SiO_2 layers are both equal to $d_1 = d_2 = 5\,\mu\text{m}$, and $N = 10$. The refractive index of SiO_2 is 2.2.

band structure is essentially not affected even in the presence of γ. The physical meaning of small bending can be seen in the Γ, R, and A spectra. Although the transmission in the first gap remains zero, the reflectance is not equal to unity because of strong absorptance there. In addition, the first gap is not due to the structural periodicity, but arises from the negative permittivity in InSb when the frequency is below the critical frequency. The second gap with a lower band edge around 4 THz is the so-called Bragg gap, which is consistent with the result of Figure 3 in Ref. [28]. It is also worthy to mention that the

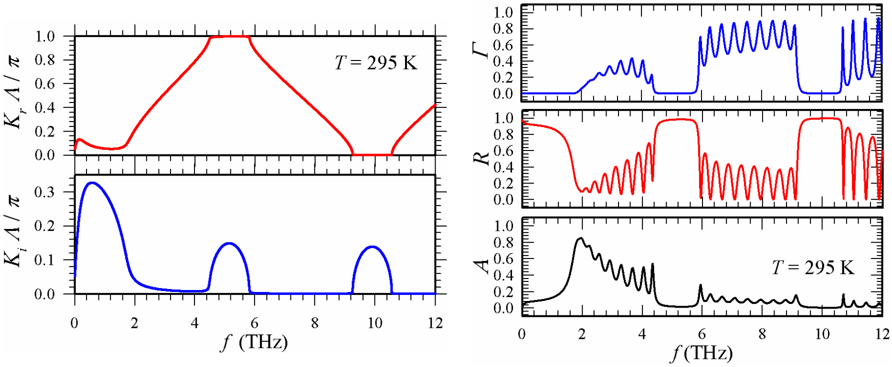

Figure 4. Calculated CPBS and Γ, R, and A at $T = 295\,\mathrm{K}$ for Air/(InSb/SiO$_2$)^N/Air. Here, the thicknesses of InSb and SiO$_2$ layers are both equal to $d_1 = d_2 = 5\,\mu\mathrm{m}$, and $N = 10$.

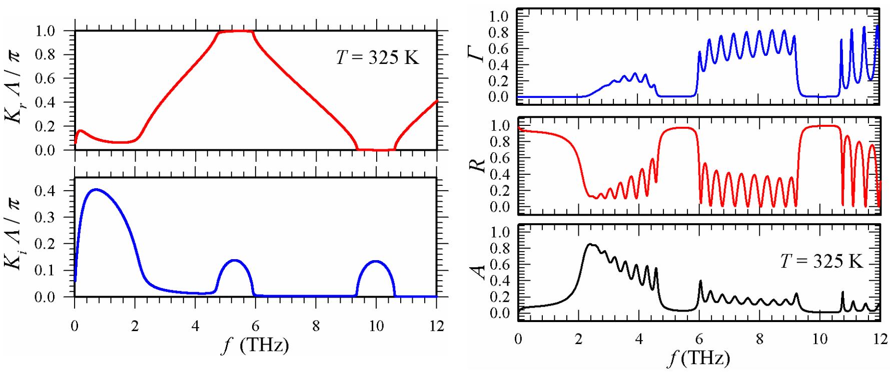

Figure 5. Calculated CPBS and Γ, R, and A at $T = 325\,\mathrm{K}$ for Air/(InSb/SiO$_2$)^N/Air. Here, the thicknesses of InSb and SiO$_2$ layers are both equal to $d_1 = d_2 = 5\,\mu\mathrm{m}$, and $N = 10$.

band edge and the gap width in the second gap cannot be estimated by usual formulas in the theory of Bragg reflector because InSb is strongly dispersive medium.

If the temperature is increased to 255 K, the CPBS is plotted in Figure 3. According to the K_r-plot, the first band gap is enlarged at 0–1 THz at this temperature. Comparing with Figure 2 reveals that the magnitude in K_i is higher than that in the second and third band gaps. Similar behavior can be seen at higher temperatures, $T = 295$, and 325 K, as shown in Figures 4 and 5, respectively. The calculated CPBSs here are in sharp contrast with those in Ref. [28], where there is no K_i and nonbending in K_r in the first band gap because the damping frequency $\gamma = 0$ has been taken.

We have so far investigated the CPBS for the SDPC at different temperatures. We now pay our attention the finite SDPC to investigate effect of damping frequency on the transmission. With the inherent damping frequency in InSb layer, it is thus worth studying the effect of number of periods. Figure 6 depicts the transmission spectrum for different number of periods at $T = 325\,\mathrm{K}$. Some features are of note. First, we define the cutoff or threshold frequency f_{th} as the starting frequency of the first transmission band, as indicated by the red arrow. It can be seen that f_{th} is slightly blue-shifted as the number of periods increases. Second, the magnitudes of the first transmission band are significantly lowered down as N increases. The magnitudes in the other transmission bands, however, are not substantially affected as N increases. This indicates that the influence of number of periods can be salient at the lower frequency transmission band when the loss is incorporated in such an SDPC. Third, in the second transmission band (near 6–9 THz), there are four peaks at $N = 5$, and nine peaks at $N = 10$. That is, there will be $N - 1$ transmission peaks at a given number of periods N. This result can be ascribed to the coupled-resonance interference mechanism [36–38]. The number of peaks is equal to the number of coupling of evanescent waves (inside the layer S) between two consecutive dielectric layers. The existence of evanescent wave in S is due to the negative permittivity at frequency lower than the plasma frequency. For example, $N = 1$, the structure is S/D, and there will no coupling (and no transmission peak) because there is only one dielectric layer D. For $N = 2$, the structure is S/D/S/D, leading to one coupling between two D's. This coupling results in a single peak. For $N = 3$, we have S/D/S/D/S/D, there are two couplings between the first two D's and between the final two D's.

This multi-peak phenomenon occurs at the frequency region below the plasma frequency (9.9 THz at 325 K). This feature enables us to design a multichannel transmission filter. The first pass band, which is far below the plasma frequency, does not have the similar trend of $N - 1$ peaks. Finally, at a sufficiently large number of periods, say $N > 30$, the first pass band is almost smeared out, leading to a very large value in f_{th}.

Finally, we fix the spatial periodicity at $\Lambda = d_1 + d_1 = 10\,\mu\mathrm{m}$ and then investigate how the transmission spectrum varies as a function of thickness ratio $\rho = d_1/d_2$. The results are shown in Figure 7. It is seen that the threshold frequency is slightly blue-shifted as ρ increases. The oscillating strength in the first transmission band is significantly decreased because of higher loss in a higher ρ-value. In addition, the

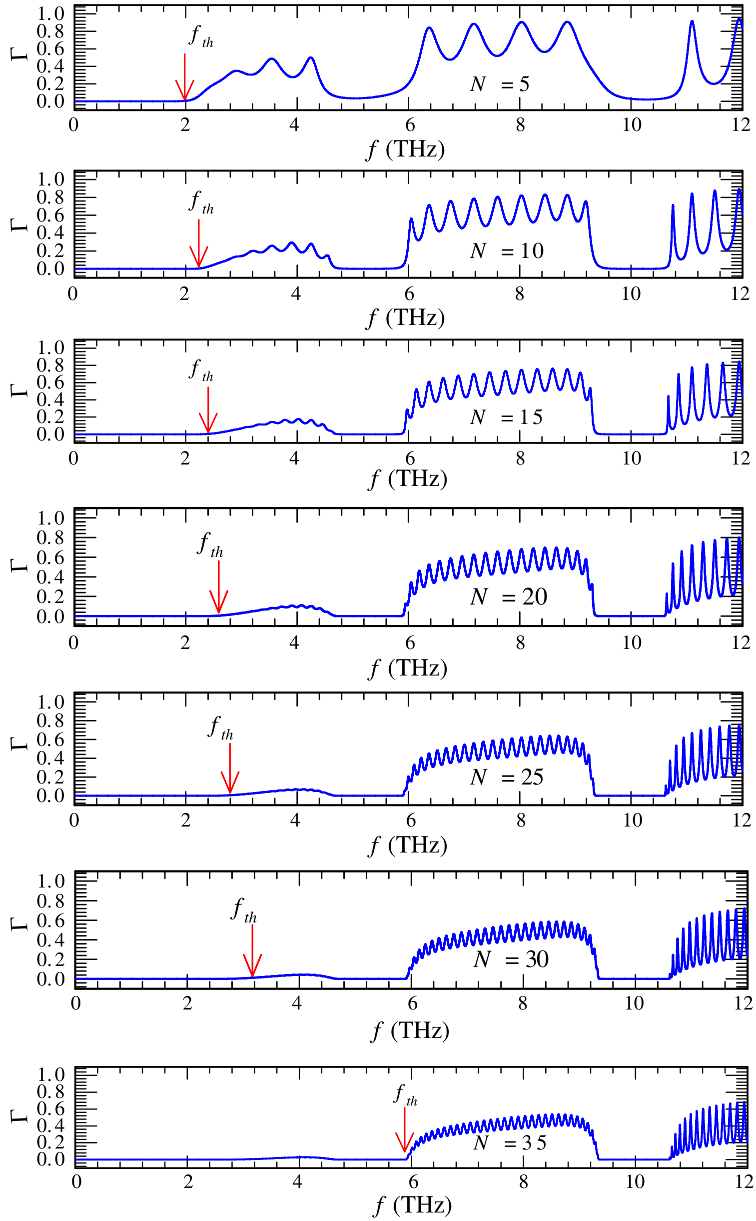

Figure 6. Calculated transmission spectra finite Air/(InSb/SiO_2)^N/Air at $T = 325\,\mathrm{K}$ at different numbers of periods Here, the thicknesses of InSb and SiO_2 layers are both equal to $d_1 = d_2 = 5\,\mu\mathrm{m}$.

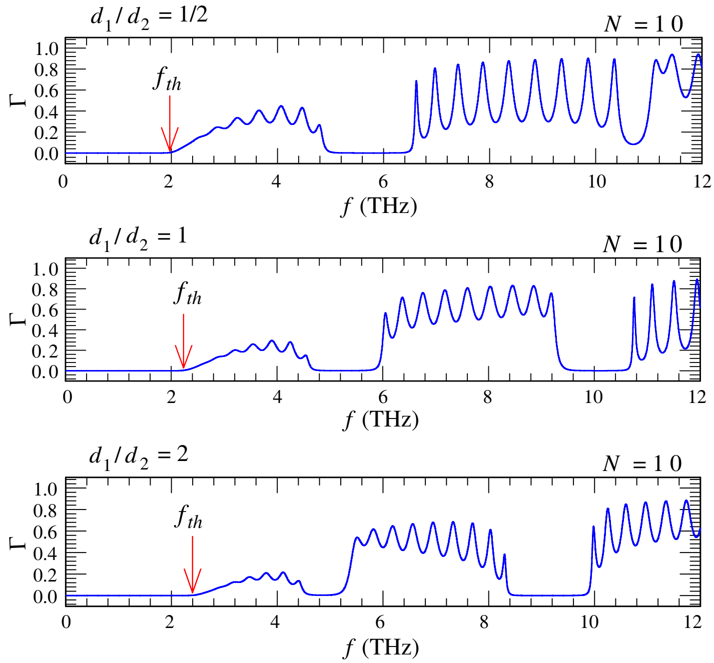

Figure 7. Calculated transmission spectra finite Air/$(InSb/SiO_2)^N$/Air at $T = 325\,\mathrm{K}$ and $N = 10$ at different numbers of thickness ratio. Here, the thicknesses of InSb and SiO_2 layers are both equal to $d_1 + d_2 = 10\,\mu\mathrm{m}$.

bandwidth of the second PBG is also reduced as ρ increases. The nine oscillating peaks in the second transmission band is squeezed and thus its bandwidth is decreased.

4. CONCLUSION

The complex photonic band structure for an InSb-SiO_2 photonic crystal has been calculated and analyzed. With the inclusion of loss factor in InSb, it is shown that the Bloch wave number is complex at the PBG and the pass band as well. The influence of the loss factor is particularly salient at the low frequency band gap and pass band. The imaginary part of complex Bloch wave number in the first band gap is enhanced as the temperature increases. Based on the calculated transmission spectrum, we have noted that, at a fixed temperature, the cutoff frequency is shifted to the higher frequency as the number of periods increases. In addition, the cutoff frequency can be slightly moved to higher frequency as the thickness ratio increases when the temperature and number of periods are fixed. The study gives some fundamental information for the semiconductor (InSb)-based photonic crystal that could be of technical use in semiconductor optoelectronics at terahertz applications.

ACKNOWLEDGMENT

C.-J. Wu acknowledges the financial support from the National Science Council of the Republic of China (Taiwan) under Contract No. NSC-100-2112-M-003-005-MY3.

REFERENCES

1. Sukhoivanov, I. A. and I. V. Guryev, *Photonic Crystals*, Springer-Verlag, Berlin, Heidelberg, 2009.
2. Orfanidis, S. J., *Electromagnetic Waves and Antennas*, Rutger University, 2008, www.ece.rutgers.edu/~orfanidi/ewa, Ch. 7.
3. Joannopoulos, J. D., R. D. Meade, and J. N. Winn, *Photonic Crystals: Molding the Flow of Light*, Princeton University Press, Princeton, NJ, 1995.
4. Li, H. and X. Yang, "Larger absolute band gaps in two-dimensional photonic crystals fabricated by a three-order-effect method," *Progress In Electromagnetics Research*, Vol. 108, 385–400, 2010.
5. Rahimi, H., A. Namdar, S. Roshan Entezar, and H. Tajalli, "Photonic transmission spectra in one-dimensional fibonacci multilayer structures containing single-negative metamaterials," *Progress In Electromagnetics Research*, Vol. 102, 15–30, 2010.
6. Chen, D., M.-L. Vincent Tse, and H.-Y. Tam, "Optical properties of photonic crystal fibers with a fiber core of arrays of subwavelength circular air holes: Birefringence and dispersion," *Progress In Electromagnetics Research*, Vol. 105, 193–212, 2010.
7. Shi, Y., "A compact polarization beam splitter based on a multimode photonic crystal waveguide with an internal photonic crystal section," *Progress In Electromagnetics Research*, Vol. 103, 393–401, 2010.
8. Mendoza-Suarez, A., H. Perez-Aguilar, and F. Villa-Villa, "Optical response of a perfect conductor waveguide that behaves as a photonic crystal," *Progress In Electromagnetics Research*, Vol. 121, 433–452, 2011.

9. Dai, X., Y. Xiang, and S. Wen, "Broad omnidirectional reflector in the one-dimensional ternary photonic crystals containing superconductor," *Progress In Electromagnetics Research*, Vol. 120, 17–34, 2011.
10. Yuan, C. P. and T.-H. Chang, "Modal analysis of metal-stub photonic band gap structures in a parallel-plate waveguide," *Progress In Electromagnetics Research*, Vol. 119, 345–361, 2011.
11. Hsu, H.-T., M.-H. Lee, T.-J. Yang, Y.-C. Wang, and C.-J. Wu, "A multichanneled filter in a photonic crystal containing coupled defects," *Progress In Electromagnetics Research*, Vol. 117, 379–392, 2011.
12. Liu, Y. and Z. Lu, "Phase shift defect modes in one-dimensional asymmetrical photonic structures consisting of two rugate segments with different periodicities," *Progress In Electromagnetics Research*, Vol. 112, 257–272, 2011.
13. Manzanares-Martinez, J., R. Archuleta-Garcia, P. Castro-Garay, D. Moctezuma-Enriquez, and E. Urrutia-Banuelos, "One-dimensional photonic heterostructure with broadband omnidirectional reflection," *Progress In Electromagnetics Research*, Vol. 111, 105–117, 2011.
14. Fink, Y., J. N. Winn, S. Fan, C. Chen, J. Michel, J. D. Joannopoulos, and L. E. Thomas, "A dielectric omnidirectional reflector," *Science*, Vol. 282, 1679–1682, 1998.
15. Winn. J. N., Y. Fink, S. Fan, and J. D. Joannopoulos, "Omnidirectional reflection from a one-dimensional photonic crystal," *Opt. Lett.*, Vol. 23, 1573–1575, 1998.
16. Kuzmiak, V. and A. A. Maradudin, "Photonic band structure of one- and two-dimensional periodic systems with metallic components in the presence of dissipation," *Phys. Rev. B*, Vol. 55, 7427–7444, 1997.
17. Contopanagos, H., E. Yablonovitch, and N. G. Alexopoulos, "Electromagnetic properties of periodic multilayers of untrathin metallic films from dc to ultraviolet frequencies," *J. Opt. Soc. Am. A*, Vol. 16, 2294–2306, 1999.
18. Bloemer, M. J. and M. Scalora, "Transmissive properties of Ag/MgF2 photonic band gaps," *Appl. Phys. Lett.*, Vol. 72, 1676–1678, 1998.
19. Choi, Y.-K., Y.-K. Ha, J.-E. Kim, H. Y. Park, and K. Kim, "Antireflection in one-dimensional metallo-dielectric photonic crystals," *Optics Communications*, Vol. 230, 239–243, 2004.
20. Halevi, P. and F. Ramos-Mendieta, "Tunable photonic crystals

with semiconducting constituents," *Phys. Rev. Lett.*, Vol. 85, 1875–1878, 2000.

21. Choudhury, P. K. and W. K. Soon, "TE mode propagation through tapered core liquid crystal optical fibers," *Progress In Electromagnetics Research*, Vol. 104, 449–463, 2010.
22. McPhail, D., M. Straub, and M. Gu, "Optical tuning of three-dimensional photonic crystals fabricated by femtosecond direct writing," *Appl. Phys. Lett.*, Vol. 87, 091117, 2005.
23. Halevi, P., J. A. Reyes-Avendano, and J. A. Reyes-Cervantes, "Electrically tuned phase transition and band structure in a liquid-crystal-infilled photonic crystal," *Phys. Rev. E*, Vol. 73, R040701, 2006.
24. Tian, H. and J. Zi, "One-dimensional tunable photonic crystals by means of external magnetic fields," *Optics Communications*, Vol. 252, 321–328, 2005.
25. Sabah, C. and S. Uckun, "Multilayer system of lorentz/drude type metamaterials with dielectric slabs and its application to electromagnetic filters," *Progress In Electromagnetics Research*, Vol. 91, 349–364, 2009.
26. Inoue, M., R. Fujikawa, A. Baryshev, A. Khanikaev, P. B. Lim, H. Uchida, O. Aktsipetrov, A. Fedyanin, T. Murzina, and A. Granovsky, "Magnetophotonic crystals," *J. Phys. D: Appl. Phys.*, Vol. 39, R151–R161, 2006.
27. Lyubchanskii, I. L., N. N. Dadoenkova, M. I. Lyubchanskii, E. A. Shapovalov, and T. Rasing, "Magnetic photonic crystals," *J. Phys. D: Appl. Phys.*, Vol. 36, R227–R287, 2003, and references therein.
28. Dai, X., Y. Xiang, S. Wen, and H. He, "Thermally tunable and omnidirectional terahertz photonic bandgap in the one-dimensional photonic crystals containing semiconductor InSb," *J. Appl. Phys.*, Vol. 109, 053104, 2011.
29. Palik, E. D., *Handbook of Optical Constants of Solids*, Elsevier, 1998.
30. Hung, H.-C., C.-J. Wu, and S.-J. Chang, "Terahertz temperature-dependent defect mode in a semiconductor-dielectric photonic crystal," *J. Appl. Phys.*, Vol. 110, 093110, 2011.
31. Meisels, R., O. Glushko, and F. Kuchar, "Tuning the flow of light in semiconductor-based photonic crystals by magnetic fields," *Photonics and Nanostructures-fundamentals and Applications*, Vol. 10, 60–68, 2012.
32. Hung, H.-C., C.-J. Wu, T.-J. Yang, and S.-J. Chang, "Magneto-

optical effect in wave properties for a semiconductor photonic crystal at near-infrared," *IEEE Photonics Journal*, Vol. 4, 903–911, 2012.

33. Howells, S. C. and L. A. Schlie, "Transient terahertz reflection spectroscopy of undoped InSb from 0.1 to 1.1 THz," *Appl. Phys. Lett.*, Vol. 69, 550–552, 1996.
34. Sanchez-Gil, J. A. and J. G. Rivas, "Thermal switching of the scattering coefficients of terahertz surface plasmon polaritons impinging on a finite array of subwavelength grooves on semiconductor surfaces," *Phys. Rev. B*, Vol. 73, 205410, 2006.
35. Yeh, P., *Optical Waves in Layered Media*, John Wiley & Sons, Singapore, 1991.
36. Feng, S., J. M. Elson, and P. L. Overfelt, "Optical properties of multilayer metal-dielectric nanofilms with all-evanescent modes," *Optics Express*, Vol. 13, 4113–4124, 2005.
37. Fang, Y.-T. and Z.-C. Liang, "Unusual transmission through one-dimensional photonic crystal in the presence of evanescent wave," *Optics Communications*, Vol. 283, 2102–2108, 2010.
38. Lin, W.-H., C.-J. Wu, T.-J. Yang, and S.-J. Chang, "Terahertz multichanneled filter in a superconducting photonic crystal," *Optics Express*, Vol. 18, 27155–27166, 2010.